REGULAR ARTICLE

Montmorillonite interlayer surface chemistry: effect of magnesium ion substitution on cation adsorption

Lasse P. Lavikainen[1] · Jukka T. Tanskanen[1] · Timothy Schatz[2] · Seppo Kasa[3] · Tapani A. Pakkanen[1]

Abstract Montmorillonite is a clay mineral and the main component in bentonite clay, which is utilized in various applications including its planned use as a buffer material for long-term nuclear waste disposal. In the present paper, a quantum chemical study is presented providing an insight into montmorillonite structure and its surface chemistry, which plays a key role in understanding montmorillonite behavior at the molecular level. A model is first designed by calculating the positions of Mg-substitutions in the octahedral sheet of the layer structure. This model is then used to study (1) charge distribution in the system and (2) the energetics of Na^+/Ca^{2+} cation adsorption on the interlayer surfaces. The results show and verify that the Mg-substitutions are positive charge deficits and the only significant charge defects in the structure. Therefore, the energetics of cation adsorption is found to correlate linearly with the inverse distances between cations and Mg-substitutions in a dry, fully periodic montmorillonite lattice.

Abbreviation
ESP   Electrostatic potential

✉ Tapani A. Pakkanen
tapani.pakkanen@uef.fi

1   Department of Chemistry, University of Eastern Finland, P.O. Box 111, 80101 Joensuu, Finland

2   B+Tech Oy, Laulukuja 4, 00420 Helsinki, Finland

3   Posiva Oy, Olkiluoto, 27160 Eurajoki, Finland

1 Introduction

Clay is a naturally occurring material, which becomes plastic when wetted and hardens when dried or fired. It is mainly composed of fine-grained minerals and other associated phases, but most importantly of clay minerals that impart to clay the aforementioned properties [1]. In bentonite clay, which is formed authigenically or by volcanic rock alteration [2], the main component is the clay mineral montmorillonite. It is responsible for the swelling behavior of bentonite when in contact with water and also provides bentonite its unique diffusive, ion exchange, mechanical and rheological properties. Consequently, montmorillonite has enabled the use of bentonite as filler, binder or absorbent/adsorbent material in various applications, including foods and beverages, water purification, catalysts, drilling mud and buffer materials. In the latter category, bentonite is the primary candidate for use as a protective release barrier for long-term nuclear waste disposal. It serves as a densely packed absorbent/adsorbent to retard the migration of pore water and possibly leaked radionuclides around waste containers [3, 4].

Montmorillonite clay mineral is a planar 2:1 phyllosilicate and belongs to the dioctahedral smectite group [5]. The planar 2:1 phyllosilicate structure is formed by one aluminum (hydr)oxide sheet, which is sandwiched between two parallel silicate sheets. On the basis of silicon or aluminum coordination numbers, the sheets are referred to as tetrahedral and octahedral, respectively. The latter may also be referred to as dioctahedral if only two of the three octahedral coordination sites are occupied. The specific characteristic that differentiates montmorillonite from other dioctahedral smectites is the appearance of isomorphic $Mg^{2+} \rightarrow Al^{3+}$ substitutions in the octahedral sheet (Fig. 1). However, finding ideal montmorillonite is unlikely
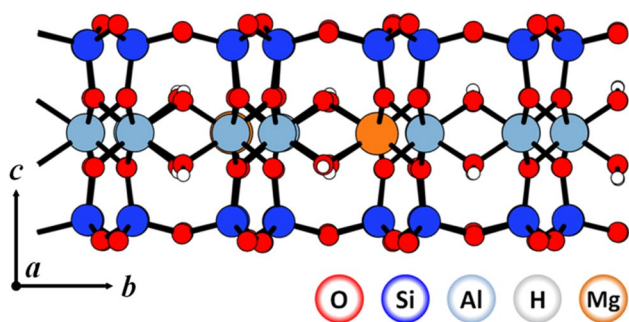
Fig. 1 Layer structure of montmorillonite

in nature, and therefore, substitutions characteristic to other smectites may also be present; commonly tetrahedral $Al^{3+}/Fe^{3+} \rightarrow Si^{4+}$ and octahedral $Fe^{2+}/Fe^{3+} \rightarrow Al^{3+}$ are observed. Due to lower charge of substituting atoms, a negative net layer charge is generated, which for smectites ranges approximately from 0.4 to 1.2 per $O_{20}(OH)_4$ formula unit [3, 6].

In the layer structure of smectites, the excess negative charge is balanced by adsorption of charge-compensating cations on the layer surfaces [7]. An electric double layer is formed, and through Coulombic interactions the layers stack into particles, which are further held together by van der Waals forces. Despite the interactions, water is able to penetrate between the layers, i.e., into the interlayer space, and hydrate the layer surfaces and the associated cations. Due to water, the layers separate further apart and the volume of the particles increases, i.e., the clay swells, rendering the interlayer cations mobile and exchangeable in the process. The extent of swelling and exchangeability depends on the layer charge and on the location of substitutions, but also on the interlayer cations: Na^+ induces greater swelling than Ca^{2+}, while poorly hydrating K^+ inhibits swelling. As for the exchange, generally, inorganic monovalent cations are exchanged for multivalent cations (e.g., Na^+ by Ca^{2+}) and smaller cations for larger cations (e.g., Na^+ by K^+) [8–14].

To obtain deeper understanding of swelling and cation exchange behavior of smectites, the interactions of cations and water with the interlayer surfaces has been examined on the molecular level. Experimental studies [15–17] are relatively few due to heterogeneous character of clay, but several theoretical studies [18–26] exist. These studies have found that the interlayer cations are present as fully or partially hydrated complexes, which interact with the layer surfaces through their hydration sphere or by direct adsorption, respectively. The type of complex is observed to depend not only on the interlayer water content and the hydration tendency of interlay cations, but also on the number and location of substitutions. Although both complex types are most often located in the vicinity of substitutions,

the probability of direct cation adsorption is highest near tetrahedral substitution sites, which locate closer to the surface compared to octahedral ones.

The cation–surface attraction due to substitutions is generally described in the literature to result from increased or localized negative charge density on the surface oxygens. While effectively correct, the exact nature of this charge has not been discussed in detail. Bleam [27] demonstrated that the negative net charge originates from a positive charge deficit, since the substitutions leave the electron count of the system unchanged, but have a lower nuclear charge compared to unsubstituted atoms in the structure. This deficit, however, cannot simply be treated as the difference between the formal charges of substituting and unsubstituted atom; some of the negative net charge may be displaced to other species due to bonding interactions. For octahedral $Mg^{2+} \rightarrow Al^{3+}$ substitutions, Bleam and Hoffmann [28] estimated with the extended Hückel method that about half of the negative net charge remains on the substitution site while the rest is deposited elsewhere in the structure, mostly on the next-nearest-neighbor aluminums.

In the present paper, we study and demonstrate the effects of octahedral Mg-substitutions in an idealized dry montmorillonite structure. Density functional theory with relaxed atomic geometries is used to verify the semiempirical charge distribution estimations of Bleam and Hoffmann. The study is then extended to investigate cation adsorption on the layer surfaces. We search for the mechanism and the relative strength of cation–surface interaction.

2 Methods and models

2.1 Computational methods

The calculations were performed with density functional theory using PBE-functional [29, 30] and projector augmented waves (PAWs) [31, 32] as implemented in the Vienna ab initio simulation package (v. 5.2.12) [33–36]. The methods have been shown to yield bond lengths for montmorillonite that are in good agreement with experimental measurements [26, 37]. Valence orbitals of all elements were described explicitly with PAWs, and additionally for group I-II elements, the lower shell $(n - 1)$ p-orbitals were included in the valance state. The kinetic energy cutoff for the basis was set to 404 eV, and only the Γ-point centered at the Brillouin zone was considered for the calculations due to the large unit cell of the system. Electronic structures were converged to 10^{-5} eV, and atomic geometries were optimized until residual forces acting on each atom were less than 0.01 eV Å^{-1}. The parameters were tested to provide accurate relative energies for the studied systems.

Charge density distribution in the montmorillonite was studied by examining electrostatic potential (ESP) and atomic charges. An ESP describes the strength of an electrostatic interaction at point of interest, and its units are equal to the work required to bring a positive charge of one elementary unit to infinite distance. The atomic charges were determined by the Bader method [38], which divides electron densities between atoms on the basis of "zero-flux surfaces" of electron density gradient, and the Voronoi (deformation density) method [39], which divides atoms and their respective electron densities on the basis of atomic geometry. The analysis of atomic charges was carried out by a third party code [40], in which the Bader atomic volumes were confined with the nearest grid method [41].

2.2 Model design

The models in the calculations were fully periodic in three dimensions. The initial model was built from *trans*-vacant pyrophyllite like unit cell with a layer symmetry c2/m and molecular formula of $Si_8Al_4O_{20}(OH)_4$. The atomic coordinates and the lattice vectors were extracted from orthogonalized montmorillonite unit cell [42] based on the electron diffraction measurements [43]. Since the unit cell did not include hydrogen atoms, they were manually added into the model. The unit cell was multiplied to create a supercell $Si_{32}Al_{16}O_{80}(OH)_{16}$ with dimensions of $2a \times 2b \times c$ in relation to the initial model. The a and b dimensions of the supercell were kept at corresponding experimental values of 10.36 and 17.96 Å, respectively, whereas the lattice vector c was fixed at 10 Å. The latter is close to experimental values obtained from dried bentonites [43] and is slightly higher than the optimized value, 9.95 Å. The fixation of the model dimensions streamlined the calculations of atomic configurations, while the choice of slightly higher c lattice vector ensured that cations have enough space to occupy the interlayer space. An exception was made in the case of atomic charge analysis for which the lattice vectors were optimized; the optimized model dimensions were 10.30 Å for a, 17.86 Å for b and 9.95 Å for c.

For addition of substitutions, montmorillonite composition data collected from Wyoming MX-80 bentonite were used as a Ref. [44]. Accordingly, the negative net layer charge of montmorillonite is approximately 0.5 per $O_{20}(OH)_4$ formula unit, and substantial amounts of octahedral Mg (~0.5) and Fe (0.36–0.38) are present in the structure along with some tetrahedral Al (0.02–0.11). The substitution densities are comparable to the data from which experimental lattice vectors were extracted for the model. However, for the purpose of the calculations reported here, Fe and Al substitutions were ignored and

only Mg-substitutions were included to generate a negative net layer charge of 0.5. This equals to two substitutions per model unit cell.

The viable positions for the Mg-substitutions in the octahedral sheet of the model unit cell were investigated. Because of the model periodicity, the addition of the first Mg-substitution was an arbitrary choice, but the position of the second one had to be calculated: 15 positions remained available. The second substitution was placed on each of these positions generating 15 different configurations. The atomic geometries of the configurations were optimized, and the total energies of the systems were examined. The lowest energy was obtained when the second substitution occupied position 5 in the substitution scheme (Fig. 2a). This configuration was set to be the reference state to which energies of other configurations were compared (Fig. 2b). The comparison indicated that several viable low-energy configurations exist and that the configurations where the substitutions occupy neighboring positions can clearly be ruled out. The second substitution was then placed on the position 6, which is next to the lowest energy position. In this way, no mirror plane was generated in the unit cell, which would reduce the number of unique cation adsorption sites on the layer surfaces. The final, substituted model having a molecular formula $Si_{32}Al_{14}Mg_2O_{80}(OH)_{16}$ is presented in Fig. 1.

(a)

(b)

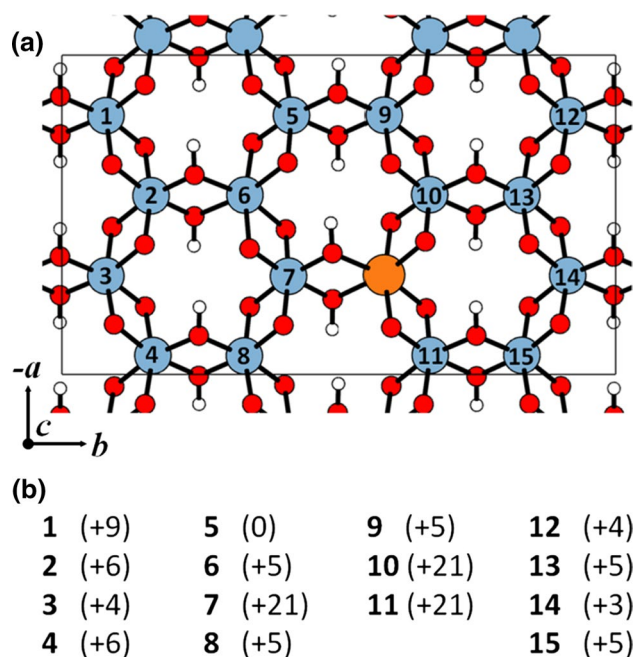|			
1 (+9)	5 (0)	9 (+5)	12 (+4)
2 (+6)	6 (+5)	10 (+21)	13 (+5)
3 (+4)	7 (+21)	11 (+21)	14 (+3)
4 (+6)	8 (+5)		15 (+5)

Fig. 2 **a** Investigated positions for the second Mg-substitution in the model. Only species in the octahedral sheet are displayed. The first arbitrarily added Mg-substitution is colored orange. **b** Relative energies (kJ mol^{-1}) for the configurations, where the second Mg-substitution is occupying one of the numbered positions

3 Results and discussion

3.1 Surface charge distribution

A qualitative examination of charge density on the model surface was first performed. ESP was mapped [45] on an electron density isosurface and on a two-dimensional plane approximately 1 Å above the surface oxygens (Fig. 3). The negative ESP maxima observed in these maps were found to be −3.3 and −9 eV, respectively, although the absolute values should be considered with
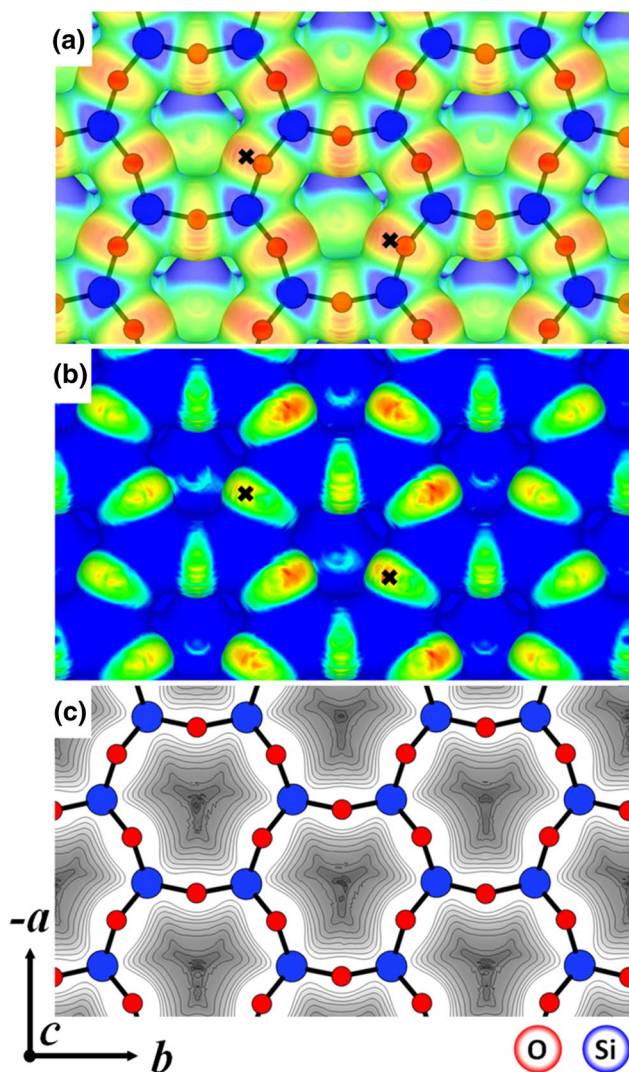

Fig. 3 ESP of montmorillonite model surface: **a** ESP mapped on an electron density isosurface. The most negative areas, up to −3.3 eV, are indicated by *red color* and positive areas by *blue color*. The *black crosses mark* positions of the Mg-substitutions in the octahedral sheet. **b** Identical to **a**, but the color scale illustrates the negative end of the potential, from −2.0 to −3.3 eV. **c** ESP mapped on a 2D-plane approximately 1 Å above the surface oxygens. The negative areas are indicated by *gray color* and positive areas by *white color*. The potential difference between *contour lines* is 1 eV

care, since they include contributions from all the layers in the periodic system.

The isosurface ESP maps indicate that the surface charge is most negative over the surface oxygens (Fig. 3a, red areas), especially in the middle area of the unit cell where the Mg-substitutions are located in the octahedral sheet (Fig. 3b, red areas). In contrast, the least negative surface oxygens are found far from the substitutions and above the hydroxyl hydrogens located in the octahedral sheet. The hydrogens can be identified as a source of positive potential (blue color) through the ditrigonal cavities of the tetrahedral sheet shown in Fig. 3a. On the other hand, what cannot be directly seen on the isosurface ESP maps but appears evident in the two-dimensional ESP map, is the negative character of ditrigonal cavity centers generated cumulatively by the surface oxygens (Fig. 3c, dark gray areas). Similar maps to Fig. 3 have been visualized in earlier studies [24, 46], but the most negative ESP could not be observed near the Mg-substitutions or in the center of ditrigonal cavities due to different models or methods.

3.2 Atomic charges

The charge distribution of the system was quantified on an atomic basis to study the origin of surface negativity. For the calculations, one Ca^{2+} cation or two Na^{+} cations were added on the model surfaces in the center of ditrigonal cavities. Both the atomic geometries and the dimensions of the model were optimized. The determination of the atomic charges was then performed by the Bader method and, for comparison, by the Voronoi method as well. In the analysis, to describe the species in different chemical environments conveniently, oxygen atoms were classified into four subtypes: bridging oxygen (ob), bridging oxygen with octahedral substitution (obos), hydroxyl oxygen (oh) and hydroxyl oxygen with substitution (ohs). The classification scheme is analogous to one used in the CLAYFF [47] force field, which is specifically parameterized for a variety of clay-type compounds. From there on, the atomic charges were calculated as an average with respect to neutral states of the atoms. The charge values in the Ca- and Na-montmorillonite models were found to be almost identical and thus are reported here solely on the basis of the Ca-montmorillonite model, except for the charge of Na. The results are presented in Fig. 4 where generalized formal charges and CLAYFF point charges are also included for comparison. A numerical presentation of the charges is included in the *supplementary information* (Online Resource 1).

The comparison of atomic charges indicates that the relative magnitudes over the different species follow a quite similar trend, despite the fact that the absolute charges vary depending on the method of determination. The trend is explained by atomic electronegativities, and therefore,
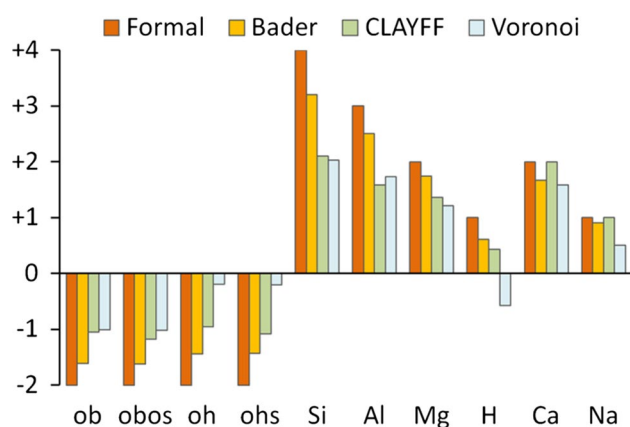
Fig. 4 Comparison of atomic charges in montmorillonite by various methods
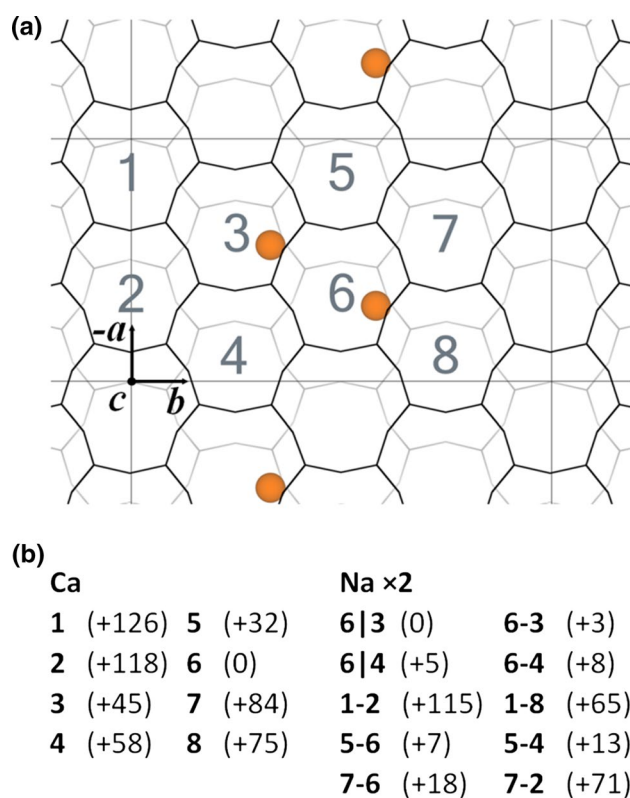

Fig. 5 **a** Ditrigonal cavity map of the montmorillonite model. The *black grid* represents the surface of the upper tetrahedral sheet (closer to the viewer) and the *gray grid* represents surface of the lower tetrahedral sheet (further from the viewer). *Numbers label* the indicated cavities of both surfaces. Except for the Mg-substitutions (*orange spheres*), the octahedral sheet has been omitted. The content of the unit cell is defined by the intersecting *gray lines*. **b** Relative energies (kJ mol^{-1}) for the configurations, where the cations are occupying cavities labelled with corresponding numbers. For Na configurations, a *bar* between numbered cavity positions indicates that cations are found on different surfaces (upper/lower), whereas a *dash* between the numbered cavity positions indicates that the cations are on the same surface

the oxygens have received electron density from electropositive Si, Al, Mg and H, as expected on the elementary basis. The only notable differences have to do with the Voronoi charges of oh, ohs and H, for which the method has assigned more electron density than the other methods. This can be explained by the geometric constraints of the Voronoi method, which by definition confines some of the electron density of relatively large oxygen into the volume of small neighboring hydrogen.

The Bader charges were further analyzed by inspecting the charge variations for each species. The range turned out to be small: approximately 0.04 for H, 0.03 for ob and $\leq$0.02 for the other species. It can be concluded that the classification scheme of the species is appropriate and that the layer charge, on atomic basis, is close to uniform along the layer. Since obos and ohs have similar charges with ob and oh, respectively, the Mg-substitutions remain as the only significant charge defects in the structure due to their lower nuclear charge; according to Bader and Voronoi charges, the Mg-substitutions are 0.76 or 0.52 elementary units less positive (more negative) than unsubstituted Al in the given order.

The results differ from the analysis of Bleam and Hoffmann [28] in a sense that the negative net charge, not localized at the Mg-substitutions, is deposited over different species in a homogeneous way. To which species and to what extent this charge is exactly being deposited remains beyond the scope of this study. The subject, however, was investigated by Voora et al. [37], who compared the atomic charge differences between pyrophyllite (no substitutions) and montmorillonite (octahedral Mg-substitutions) with similar methods. According to their calculations, the excess negative net charge, introduced by the addition of the Mg-substitutions, is mainly being deposited on the surface oxygens. Although their model unit cell had slightly different Mg-substitution distribution and was half of the size employed here, their results for montmorillonite are in close agreement with this study.

3.3 Energetics of interlayer cation adsorption

Charge deficits at the Mg-substitution sites can be viewed as the source of a negative net electrostatic potential and therefore are expected to affect the interaction of interlayer cations with the layer surfaces. The correlation of this potential on cation adsorption energetics was studied by varying the positions of Ca^{2+} and Na^{+} cations on the layer surfaces, also taking into account the relaxation of atomic geometries. The studied models included one Ca^{2+} or two Na^{+} cations to compensate for the total layer charge of the model. The cations were placed in ditrigonal cavities, knowing that (1) the ESP, as seen in Fig. 3c, has high negativity in the center of each cavity, (2) optimization
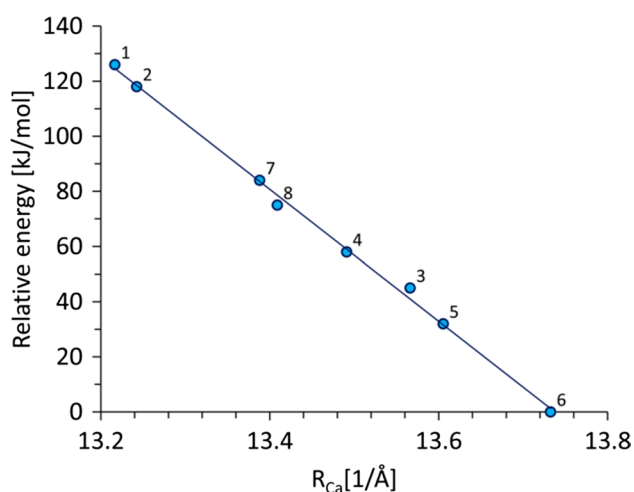
Fig. 6 Correlation of relative Ca^{2+} cation adsorption energetics with R_{Ca}. *The labels* indicate cation adsorption sites as defined in Fig. 5

Fig. 7 Correlation of relative Na^+ cation adsorption energetics with R_{Na}. *The labels* indicate cation adsorption sites as defined in Fig. 5

algorithm tends to move the cations into cavities even with higher layer spacings and (3) there is not much space for cations to locate elsewhere between dry, tightly stacked montmorillonite layers [37].

In the model unit cell, both of the layer surfaces have similar geometry and eight cavities (Fig. 6a). These cavities can be occupied by one Ca^{2+} cation in eight unique configurations, whereas two Na^+ cations can occupy the cavities of both layer surfaces in a much greater number of permutations. For Ca^{2+} cation, all the unique configurations were studied, but for Na^+ cations the number of configurations was limited to few different ones. When the atomic geometries of the configurations were optimized, the cations slightly shifted toward the Mg-substitutions either parallel to the surface (in cavities 3, 4, 7 and 8) or along the surface normal (in cavities 5 and 6). Some of the smaller Na^+ cations (in cavities 1, 2 and 7) shifted out of the cavities along the a/c-direction and located between the layer surfaces, but the rest of the cations remained in the cavities. Also changes in cavity geometries were observed as the oxygen atoms moved in for closer contact with the cations.

The energetics of the optimized configurations was analyzed in an analogous way to Mg-substitution configurations, as described in the *methods and models* section. The results (Fig. 6b) revealed that energy differences between the cation-associated configurations are significant, up to 126 kJ mol^{-1}, and the lowest energies are obtained when the cations occupy cavities closest to the Mg-substitutions. Clearly, the Mg-substitutions have a major impact on the cation–surface interaction. The dependence of the cation adsorption energetics on the cation-substitution distance is presented in Figs. 6 and 7, where the relative configuration energies are plotted against the sum of inverse cation-substitution distances, R_{Ca} and R_{Na}. For the calculations of
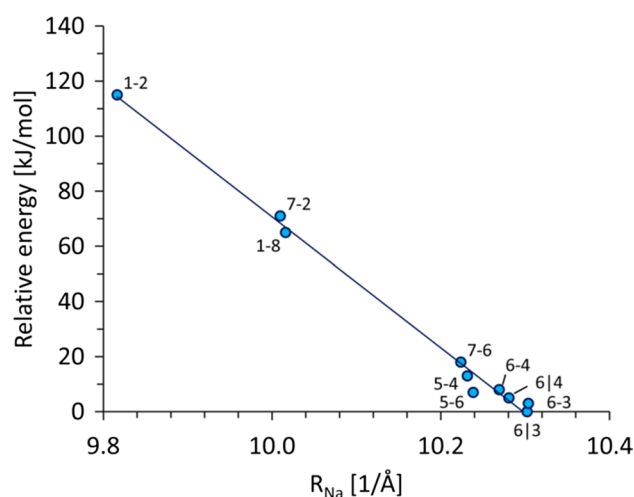
R_{Ca} and R_{Na}, see the *supplementary information* (Online Resource 1).

As seen in the Figs. 6 and 7, the relative energies of the cation-associated configurations are linearly well correlated ($r^2 > 0.99$) with the sums of inverse cation-substitution distances; the slopes are -239.1 kJ Å mol^{-1} for Ca^{2+} systems and -237.6 kJ Å mol^{-1} for Na^+ systems. The negativity of the slopes indicates attractive cation–surface interaction which increases as the effective distance between cations and Mg-substitutions decreases. In other words, the energetics of cation–surface interaction is inversely proportional to the distance between cations and Mg-substitutions in the periodic three-dimensional lattice.

The results can be viewed as an extension to the study of Bleam [27], who used a two-dimensional array of fixed point charges to demonstrate that the potential above substitutions are linear along the surface normal but curves close to the surface due to the potential of the tetrahedral sheet. In Figs. 6 and 7, no curving is observed, since the potential generated by the tetrahedral sheet is approximately constant on the level of adsorbed cations. The calculations presented here thereby confirm that the octahedral Mg-substitutions can be treated as a negative point-like charge defects in the montmorillonite structure. Although in natural systems and technological applications, the cation–surface interaction is further complicated by the effects of interlayer water, i.e., hydration, swelling and dielectric screening; the interactions presented here, even if reduced, should remain.

4 Conclusions

Montmorillonite structure and interlayer surface chemistry were studied by quantum chemical methods. The

surface electrostatic potential, which qualitatively predicts the most probable adsorption sites for interlayer cations, was observed to be most negative near the octahedral Mg-substitutions. According to calculated atomic charges, this negativity originates from the Mg-substitutions which are positive charge deficits and the only significant charge defects in the layer structure. The energetics of Ca^{2+} and Na^+ cation adsorption on the layer surfaces was found to correlate linearly with the inverse cation-substitution distances, thus confirming the negative point-like character of the Mg-substitutions. The variations in cation adsorption energies were notable, up to 126 kJ mol^{-1}, with respect to different adsorption sites in the model.

The results help to understand and verify the nature of negatively charged montmorillonite surfaces. The surface charge is a fundamental property affecting hydration, swelling and cation migration/exchange behavior of montmorillonite, which have a central role in bentonite buffer applications, e.g., isolation of radionuclides in long-term nuclear waste disposal. The results may be used in molecular dynamic studies to evaluate energetics of the system and to interpret the behavior of cationic species in the interlayer space of montmorillonite or other similar phyllosilicates.

References

1. Guggenheim S, Martin RT (1995) Clays Clay Miner 43:255–256
2. Galán E (2006) In: Bergaya F, Theng BKG, Lagaly G (eds) Developments in clay science, vol 1, 1st edn. Elsevier Ltd, Oxford, pp 1153–1154
3. Přikryl R (2006) In: Al-Rawas AA, Goosen MFA (eds) Expansive soils: recent advances in characterization and treatment. Taylor & Francis Group, London, pp 40–49
4. Pusch R (1992) Clay Miner 27:353–361
5. Guggenheim S, Adams JM, Bain DC, Bergaya F, Brigatti MF, Drits VA, Formoso MLL, Galán E, Kogure T, Stanjek H (2006) Clays Clay Miner 54:761–772
6. Brigatti MF, Galán E, Theng BKG (2006) In: Bergaya F, Theng BKG, Lagaly G (eds) Developments in clay science, 1st edn. Elsevier, Oxford, vol 1, pp 19–24, 41–43
7. Schoonheydt RA, Johnston CT (2006) In: Bergaya F, Theng BKG, Lagaly G (eds) Developments in clay science, vol 1, 1st edn. Elsevier, Oxford, pp 87–89
8. Lagaly G (2006) In: Bergaya F, Theng BKG, Lagaly G (eds) Developments in clay science, 1st edn. Elsevier, Oxford, vol 1, pp 141–152, 247–257
9. Pusch R (2006) In: Bergaya F, Theng BKG, Lagaly G (eds) Developments in clay science, vol 1, 1st edn. Elsevier, Oxford, pp 247–257
10. Laird DA (2006) Appl Clay Sci 34:74–87
11. Weir AH (1965) Clay Miner 6:17–22
12. Onodera Y, Iwasaki T, Ebina T, Hayashi H, Torii K, Chatterjee A, Mimura H (1998) J Contam Hydrol 35:131–140
13. Bergaya F, Lagaly G, Vayer M (2006) In: Bergaya F, Theng BKG, Lagaly G (eds) Developments in clay science, vol 1, 1st edn. Elsevier, Oxford, pp 979–987
14. Rotenberg B, Morel J, Marry V, Turq P (2009) Geochim Cosmochim Acta 73:4034–4044
15. Skipper NT, Soper AK, Smalley MV (1994) J Phys Chem 98:942–945
16. Skipper NT, Smalley MV, Williams GD (1995) J Phys Chem 99:14201–14204
17. Slade PG, Stone PA, Radoslovich EW (1985) Clays Clay Miner 33:51–61
18. Boek ES, Coveney PV, Skipper NT (1995) J Am Chem Soc 117:12608–12617
19. Chang FRC, Skipper NT, Sposito G (1995) Langmuir 11:2734–2741
20. Chang FRC, Skipper NT, Sposito G (1997) Langmuir 13:2074–2082
21. Chang FRC, Skipper NT, Sposito G (1998) Langmuir 14:1201–1207
22. Greathouse J, Sposito G (1998) J Phys Chem B 102:2406–2414
23. Sposito G, Skipper NT, Sutton R, Park S, Soper AK, Greathouse JA (1999) Proc Natl Acad Sci 96:3358–3364
24. Mignon P, Ugliengo P, Sodupe M, Hernandez ER (2010) Phys Chem Chem Phys 12:688–697
25. Suter JL, Boek ES, Sprik M (2008) J Phys Chem C 112:18832–18839
26. Berghout A, Tunega D, Zaoui A (2010) Clays Clay Miner 58:174–187
27. Bleam WF (1990) Clays Clay Miner 38:527–536
28. Bleam WF, Hoffmann R (1988) Inorg Chem 27:3180–3186
29. Perdew JP, Burke K, Ernzerhof M (1996) Phys Rev Lett 77:3865–3868
30. Perdew JP, Burke K, Ernzerhof M (1997) Phys Rev Lett 78:1396
31. Blöchl PE (1994) Phys Rev B 50:17953–17979
32. Kresse G, Joubert D (1999) Phys Rev B 59:1758–1775
33. Kresse G, Hafner J (1993) Phys Rev B 47:558–561
34. Kresse G, Hafner J (1994) Phys Rev B 49:14251–14269
35. Kresse G, Furthmüller J (1996) Comput Mater Sci 6:15–50
36. Kresse G, Furthmüller J (1996) Phys Rev B 54:11169–11186
37. Voora VK, Al-Saidi W, Jordan KD (2011) J Phys Chem A 115:9695–9703
38. Bader R (1990) In: Atoms in molecules: a quantum theory. Oxford University Press, Oxford
39. Fonseca Guerra C, Handgraaf J, Baerends EJ, Bickelhaupt FM (2004) J Comput Chem 25:189–210
40. Arnaldsson A, Tang W, Chill S, Henkelman G, Sanville E, Voss J, McNellis E, Dyer M, Lebegue S, Janos A, Aubert E. Code: Bader charge analysis, v. 0.28a, 2012
41. Tang W, Sanville E, Henkelman G (2009) J Phys Condens Matter. doi:10.1088/0953-8984/21/8/084204
42. Viani A, Gualtieri AF, Artioli G (2002) Am Miner 87:966–975
43. Tsipursky SI, Drits VA (1984) Clay Miner 19:177–193
44. Karnland O, Olsson S, Nilsson U (2006) SKB-report: mineralogy and sealing properties of various bentonites and smectite-rich clay materials, TR-06-30
45. Momma K, Izumi F (2011) J Appl Crystallogr 44:1272–1276
46. Gorb L, Gu J, Leszczynska D, Leszczynski J (2000) Phys Chem Chem Phys 2:5007–5012
47. Cygan RT, Liang J-, Kalinichev AG (2004) J Phys Chem B 108:1255–1266